Establishment of beta cell heterogeneity via differential CpG methylation at *Nnat*

Vanessa Yu[1], Fiona Yong[1,2], Keran Chen[1], Eleni Georgiadou[1], Nazia Parveen[3], Angellica Marta[1], Sanjay Khadayate[4], Zoe Stamoulis[1], Lorella Marselli[5], Carmela De Luca[5], Mara Suleiman[5], Yuki Hatanaka[4], Alex Montoya[4], James Elliott[4], Bhavik Patel[4], Nikita Demchenko[4], Chad Whilding[4], Petra Hajkova[4], Pavel Schliaha[4], Holger Kramer[4], Yusuf Ali[6-8], Piero Marchetti[5], Sangeeta Dhawan[3], Dominic J. Withers[4], Guy A. Rutter[1,2,9]* and Steven J. Millership[1]*

[1]Section of Cell Biology and Functional Genomics, Department of Metabolism, Digestion and Reproduction, Faculty of Medicine, Imperial College London, Du Cane Road, London, W12 0NN, UK

[2]Lee Kong Chian School of Medicine, Nanyang Technological University, 637553, Singapore

[3]Department of Translational Research and Cellular Therapeutics, Arthur Riggs Diabetes and Metabolism Research Institute, City of Hope, 1500 E Duarte Road, Duarte, CA 91010, USA

[4]MRC London Institute of Medical Sciences, Du Cane Road, London, W12 0NN, UK

[5]Department of Clinical and Experimental Medicine, and AOUP Cisanello University Hospital, University of Pisa, Pisa 56126, Italy

[6]Nutrition, Metabolism and Health Programme & Centre for Microbiome Medicine, Lee Kong Chian School of Medicine, Nanyang Technological University Singapore, Singapore, 308232

[7]Singapore Eye Research Institute (SERI), Singapore General Hospital, Singapore, 168751

[8]Clinical Research Unit, Khoo Teck Puat Hospital, National Healthcare Group, Singapore, 768828

[9]CHUM Research Center and Faculty of Medicine, University of Montréal, 900 Rue St Denis, Montréal, H2X OA9, QC, Canada

*Corresponding authors, e-mail: s.millership@imperial.ac.uk; g.rutter@imperial.ac.uk

Abstract

Beta cells within the pancreatic islet represent a heterogenous population wherein individual sub-groups of cells make distinct contributions to the overall control of insulin secretion. The molecular mechanisms through which beta cell hierarchy is established remain poorly understood. The neuronatin (*Nnat*) gene is imprinted in mice and humans and is required for normal insulin synthesis and secretion. Here, we demonstrate that *Nnat* is differentially expressed in a discrete beta cell population in a developmental-stage and DNA methylation (DNMT3A)-dependent manner. Explored in mice expressing eGFP from a bacterial artificial chromosome-expressed transgene, NNAT$^+$ cells displayed a discrete transcriptome, and appear to represent a beta cell population specialised for insulin production. Correspondingly, highly connected 'hub' cells were less abundant in the NNAT$^+$ population. These findings

demonstrate that differential DNA methylation at *Nnat* represents a novel means through which beta cell heterogeneity is established.

Key words: beta cell heterogeneity; CpG methylation; imprinted genes; neuronatin; type 2 diabetes; beta cell development; beta cell identity.

Introduction

Insulin-producing beta cells are central to the modulation of glucose homeostasis and their impaired function, loss of identity, or lowered numbers result in type 2 diabetes (T2D) (1, 2). Previous studies have provided us with an understanding of the transcriptional machinery that orchestrates beta cell development from early pancreatic and endocrine precursors (3-6). To bolster these transcriptional programmes *in vivo*, chronic regulation via the epigenome appears to step in to maintain beta cell identity in the long term (7-15).

Earlier reports (16-19), and more recent studies based on single cell transcriptomic profiling (20-22), electrophysiology (23) and functional imaging (24-27) have demonstrated functional heterogeneity amongst individual beta cells within pancreatic islets (reviewed in (28, 29)). Identified subpopulations of beta cells have been associated with known markers or maturation states (*Flattop*/*Cfap126* (26), PSA-NCAM (30), *Cd81* (31), CD24 (32), TH (15), NPY (33)) are 'virgin' beta cells (34) or can be defined in terms of their roles in coordinating islet-wide Ca^{2+} dynamics (e.g. 'hubs' (24) and 'leaders' (25, 35, 36)). Furthermore, loss of beta cell heterogeneity or intercellular connectivity may contribute to the development of T2D (24, 25, 37-39). Importantly, functional subpopulations have also been demonstrated in human beta cells (21, 22, 40-42), where antigenically-defined human beta cells (by CD9 and ST8SIA1) have been shown to have an altered subtype distribution in T2D (20). The features underlying beta cell heterogeneity involve differences in pathways governing glucose sensing and metabolism (24-26, 30, 43, 44) insulin content and secretory competence (14, 23, 34, 45, 46) cilia activity and localisation vis-à-vis other endocrine cell types (36). However, the molecular control that leads to the establishment, and long-term maintenance, of higher orders of beta cell subtypes are poorly defined. Changes at the level of the epigenome provides one such possibility.

Imprinted genes are expressed from a single allele in a parent of origin-specific manner. The expression of these genes is controlled via epigenetic modifications, particularly through DNA methylation (47). Imprinted genes often play key physiological roles, particularly in early (fetal and postnatal) growth and development, controlling a wide range of cellular processes (48, 49). Human imprinting disorders involving altered expression from specific imprinted *loci* are associated with severe childhood developmental and metabolic complications, demonstrating the need for tightly controlled imprinted gene expression (50, 51). Imprinted genes play key functional roles in pancreatic beta cells by modulating insulin secretory machinery or beta cell mass (52). Correspondingly, imprinted gene expression is deregulated in both beta cells with diminished glucose-stimulated insulin secretion (GSIS) (53) and in pancreatic islets from subjects with T2D (54-59). Furthermore, single nucleotide polymorphisms (SNPs) at imprinted

loci are associated with T2D, possibly due to altered methylation at these genomic regions (60). Importantly, dietary excess (high fat or high sugar diets) is linked to long-term, programmed epigenetic changes at imprinted *loci* in humans and rodents (61-63). Epigenetic control of imprinted gene expression is predominantly regulated by DNA methylation at cytosine-guanine rich CpG 'islands', with monoallelic expression maintained transgenerationally by differential methylation between parental alleles at imprinted *loci* in the germline (64, 65). However, and in addition to differentially methylated regions (DMRs) in gametes, 'somatic' or 'secondary' DMRs can also be established post-fertilisation, and provide an additional layer of control (66).

We have shown previously (67) that the paternally expressed, imprinted gene *Neuronatin* is nutrient-regulated in pancreatic beta cells, and controls insulin content and therefore glucose-stimulated insulin secretion (GSIS). *Nnat* action involves modulating early insulin precursor processing via augmentation of the signal peptidase complex (67). At extra-pancreatic sites, changes in *Nnat* expression in rodents and humans also modulate appetite, energy expenditure, body weight and adipose tissue mass (68-71). Here, we show that differential methylation of the *Nnat* gene contributes to the functional heterogeneity of adult pancreatic beta cells.

Materials and Methods

Animal models

All animal procedures were in accordance with the UK Animals (Scientific Procedures) Act 1986 and approved by both the UK Home Office (PPL: PP4712156) and the Imperial College Animal Welfare and Ethical Review Body. Animals were euthanised by cervical dislocation. Animal work was designed and reported according to the Animal Research: Reporting of In Vivo Experiments (ARRIVE) guidelines. Power calculations were based on known effect sizes. Where possible, blinding for experimental mice and tissues was used and all studies were replicated in at least three independent cohorts or using litters from three different breeding cages.

Transgenic mice lines expressing *Cre* recombinase under the control of the rat insulin promoter (RIP) (72) and with a tdTomato reporter downstream of a stop codon flanked by *loxP* sites (73) have been described previously. Mice with *Nnat*-driven *Egfp* expression were purchased from the Mutant Mouse Resource and Research Centre (MMRRC) repository (Tg(Nnat-EGFP)EA106Gsat/Mmucd, #010611-UCD) with the presence of the *Egfp* allele assessed by standard PCR using DNA from ear biopsy (primers 5'-

CATCACCCCTCCTTCTCAAC-3' and 5'-GAACTTCAGGGTCAGCTTGC-3'). Mice with global deletion of *Nnat* were used as previously described (67). Conditional *Dnmt3a* null mice (74), generated by crossing to *Pdx1-Cre* (75) have been described elsewhere (13, 15, 76). Mice containing the *Dnmt3a* floxed allele but lacking *Pdx1-Cre* were used as controls. All mice were on a C57BL/6J background and experimental cohorts were group-housed and maintained on a 12-hour light/dark cycle. Animals were fed standard mouse chow (RM3, Special Diet Services) with access to drinking water *ad libitum* in specific pathogen-free barrier facilities. Male mice were 10-12 weeks old at the time of experiments unless otherwise stated. For experiments involving the *Nnat*-eGFP reporter line, mice were hemizygous for the reporter via paternal transmission, unless otherwise stated. Sperm was isolated from young adult male C57BL/6J mice.

Primary islet isolation, glucose-stimulated insulin secretion (GSIS) and fluorescence-activated cell sorting (FACS).

To isolate primary islets, the pancreas was inflated with Liberase TM (Roche), digested at 37°C, purified using a Histopaque 1119/1083/1077 gradient (Sigma-Aldrich) and hand-picked. For FACS-based experiments, single cells from purified islets were isolated using Accutase (Sigma-Aldrich) for 5 min. at 37°C followed by gentle disaggregation by pipetting. Islet cells were centrifuged and resuspended in FACS buffer (25 mM HEPES, 5 mM EDTA, 1% fetal bovine serum (FBS) in PBS, pH 7.4) prior to cell sorting using an FACSAria III flow cytometer (BD) equipped with 488 nm and 561 nm lasers for excitation of EGFP and tdTomato, respectively. Emission from EGFP and tdTomato expressing cells was collected using a 530/30 and 580/30 bandpass filter, respectively. Forward scatter area vs forward scatter height was used to offset and remove doublets.

Intracellular calcium imaging

Pancreatic islets were isolated as above and left to settle overnight in RPMI (Gibco) supplemented with 10% (v/v) FBS, (Sigma-Aldrich), 2 mM L-glutamine and 100 U/mL penicillin/100 μg/mL streptomycin (both Gibco) at 37°C and 5% CO_2. Ca^{2+} imaging of whole islets was performed after loading the cytosol with 2 μM Cal-590 AM (Stratech) in Krebs-Ringer bicarbonate buffer (140 mM NaCl, 3.6 mM KCl, 0.5 mM NaH_2PO_4, 2 mM $NaHCO_3$ (saturated with CO_2), 1.5 mM $CaCl_2$, 0.5 mM $MgSO_4$, 10 mM HEPES, pH 7.4) containing 3 mM or 11 mM glucose. Images were captured at 0.5 Hz on an Axiovert microscope (Zeiss) equipped with a 10x 0.3–0.5 NA objective, a Hamamatsu ImagEM camera coupled to a Nipkow spinning-disk head (CSU-10, Yokogawa) and illuminated at 490 nm or 530 nm. Data were analysed using ImageJ and changes in fluorescence intensity over time

were measured after drawing ROI's around individual cells for each islet. Pearson-based connectivity and correlation analyses were performed as previously described (77). The first 50 datapoints were removed to account for the initial spike in response to the addition of 11 mM glucose. Signal binarisation-based connectivity and correlation analyses were performed as previously described (36). Connectivity between cells was explored using Pearson's R-based correlation analyses in MATLAB as described (76). We note that although the Ca^{2+} dye used here was not selectively targeted towards beta cells, at the concentration of glucose used (11 mM), pancreatic alpha cells are expected to be largely inactive. We do not exclude a contribution of delta cells, although these represent <5% of the overall endocrine cell population.

Histological techniques and immunofluorescence

Dissected tissues were fixed in 4% paraformaldehyde at 4°C, washed with PBS and cryoprotected overnight at 4°C using 30% (w/v) sucrose in PBS before embedding in OCT and stored at -80°C. Sections (10 μm) were cut using a CM1950 Cryostat (Leica) and permeabilised with 0.2% Triton X-100 in PBS, followed by blocking in 2% (w/v) BSA and 5% (v/v) chicken serum in PBS containing 0.1% Tween-20. Sections were immunostained using primary antibodies diluted in blocking buffer against NNAT (clone EPR13554(B), ab181353 from Abcam, 1:1000), GFP (GFP-1010, Aves Labs, 1:3000) INS (I2018, Sigma-Aldrich, 1:5000), somatostatin (SST) (American Research Products, 13-2366, 1:1000), GCG (clone C-18, sc-7779, Santa Cruz Biotechnology, 1:50), DNMT1 (60B1220.1, Novus Biologicals, 1:500) and DNMT3A (64B1446, Novus Biologicals, 1:500) with overnight incubation at 4°C followed by incubation with secondary antibody (Alexa Fluor, Thermo Fisher Scientific, 1:500). Sections were imaged using a TCS SP5 confocal microscope (Leica). Immunostaining of paraffin-embedded pancreas from mice with beta cell-selective deletion of *Dnmt3a* was performed according to (15, 33, 78) using antibodies against NNAT (ab27266, Abcam, 1:200) and INS (ab195956, Abcam, 1:800). Cell classification was carried out with a custom-written Fiji script (79) and CellProfiler pipeline (software version 4.1.3). Nuclei segmentation was batch processed in Fiji using the Stardist plugin, with subsequently generated nuclei label images imported into CellProfiler for cell type classification following measurement of fluorescence intensity in acquired fluorescent channels.

Cell culture, RNA silencing and GSIS

Human EndoC-βH1 (80) and rat INS1E (81) beta cells were cultured as previously described (67). EndoC-βH1 beta cells were incubated with lentiviruses expressing an *NNAT*-targeting shRNA (clone ID: TRCN0000163961) *vs* scrambled shRNA control (multiplicity of infections

(MOI) = 2, MISSION transduction particles, Sigma-Aldrich) for 72h in complete media without BSA. INS1E cells were transfected with Silencer Select siRNAs (30 nM; *Nnat*, s137247; *Sec11a*, s80747; *Spcs1*, s226238; *Spcs2*, s18919; *Spcs3*, s184336; all Ambion) using Lipofectamine 2000 (Invitrogen) in optiMEM (Gibco) for 48h. GSIS assays were performed as previously described (80). Briefly, EndoC-βH1 cells were cultured in low (2.8 mM) glucose complete media for 16h prior to GSIS assay. Cells were incubated in Krebs-Ringer bicarbonate buffer (115 mM NaCl, 5 mM KCl, 24 mM $NaHCO_3$ (saturated with CO_2), 1 mM $CaCl_2$, 1 mM $MgSO_4$, 10 mM HEPES, 0.2% BSA, pH 7.4) containing 0.5 mM glucose for 1h prior to incubation with low (3 mM) or high (16.7 mM) glucose for 1h. Cells were collected in lysis buffer (20 mM Tris-HCl pH 7.5, 137 mM NaCl, 0.1% Triton X-100, 2 mM EGTA, 1% glycerol with protease inhibitors (Complete Mini from Roche)), centrifuged for 5 min at 3,000 rpm and 4°C, with supernatants and collected media stored at -80°C until insulin quantification with ultra-sensitive insulin homogeneous time-resolved fluorescence (HTRF) assay kits (Cisbio).

Immunoprecipitation and mass spectrometry

Cells were homogenised in protein lysis buffer (50 mM Tris-HCl pH 7.5, 150 mM NaCl, 1% Triton X-100, 1 mM EDTA with protease inhibitors, Complete Mini from Roche), solubilised for 30 min. on ice, clarified and normalised for protein content. Supernatants were incubated with protein A-agarose beads (Calbiochem) and antibodies against NNAT (ab27266, Abcam, 1:500) or rabbit IgG overnight at 4°C. Agarose beads were washed seven times with protein lysis buffer, with the final three washes not containing Triton X-100. For mass spectrometry, beads were sedimented and resuspended in 100 μL of 20 mM HEPES (pH 8.0), 1M urea, 1 mM dithiothreitol (DTT) and 1.5 μg of trypsin gold (Promega) overnight at 37 °C. Digests were subsequently acidified with trifluoroacetic acid, followed by de-salting using reversed-phase spin tips (Glygen Corp) according to the manufacturer's recommendations. Eluents were subsequently dried to completion using vacuum centrifugation. Dried peptides were re-suspended in 0.1% trifluoroacetic acid (TFA) and analysed by LC-MS/MS analysis using an Ultimate 3000 nano-HPLC coupled to a Q-Exactive mass spectrometer (Thermo Scientific) via an EASY-Spray source. Peptides were loaded onto a trap column (Acclaim PepMap 100 C18, 100μm × 2cm) at 8 μL/min in 2% acetonitrile, 0.1% TFA. Peptides were then eluted on-line to an analytical column (Acclaim Pepmap RSLC C18, 75 μm × 75 cm). A stepped gradient separation was used with 4-25% of 75% acetonitrile, 0.1% formic acid for 75-90 min, followed by 25-45% for 10-30 min, with subsequent column conditioning and equilibration. Eluted peptides were analysed by the Q-Exactive operating in positive polarity and data-dependent acquisition mode. Ions for fragmentation were determined from an initial MS1 survey scan at

70000 (EndoC-βH1) or 120,000 resolution (INS1E), followed by HCD (Higher-energy collisional dissociation) of the top 12 (EndoC-βH1) or 20 (INS1E) most abundant ions at a resolution of 17,500 (EndoC-βH1) or 15,000 (INS1E). MS1 and MS2 scan AGC targets set to 3e6 and 5e4 for a maximum injection time of 50ms and 50ms (EndoC-βH1) and 25ms and 110ms (INS1E), respectively. A survey scan m/z range of 400–1800 m/z (EndoC-βH1) or 350-1750 (INS1E) was used, with a normalised collision energy set to 27%, minimum AGC of 1e3, charge state exclusion enabled for unassigned and +1 ions and a dynamic exclusion of 30 (EndoC-βH1) or 50 (INS1E) seconds. Data was processed using the MaxQuant (82) software platform (v1.6.1.0) for EndoC-βH1 and (v1.6.10.43) for INS1E with database searches carried out by the in-built Andromeda search engine against the Swissprot Homo Sapiens database (downloaded 4th January 2018, entries: 20,256) or Ratttus Norvegicus (Downloaded 31st May 2022, entries: 22,831). A reverse decoy database approach was used at a 1% FDR for peptide spectrum matches and protein identifications. Search parameters included: maximum missed cleavages set to 2, variable modifications of methionine oxidation, protein N-terminal acetylation, asparagine deamidation and cyclisation of glutamine to pyroglutamate. Label-free quantification was enabled with an LFQ minimum ratio count of 2 (EndoC-βH1) or 1 (INS1E).

Western immunoblotting, RT-PCR, RNA sequencing

For Western blotting, EndoC-βH1 cells were homogenised in protein lysis buffer as above, clarified and normalised for protein content using the BCA method (Bio-Rad) as previously described (67). Briefly, proteins were transferred from SDS-PAGE to PVDF and immunoblotted using antibodies against NNAT (ab27266, Abcam, 1:2000) and β-tubulin (clone 9F3, Cell Signalling, 1:5000), HRP-conjugated secondary antibodies (Cell Signalling, 1:3000) and Immobilon Forte Western HRP substrate (Millipore). Scanned blots were assessed by densitometry using Image J. For RT-PCR, mRNA was purified using an Allprep DNA/RNA/protein mini kit or by direct homogenisation into Trizol reagent with purification using chloroform and RNeasy kits (both Qiagen). Normalised quantities of mRNA were reverse transcribed, and cDNA assessed by quantitative RT-PCR using Taqman reagents on a QuantStudio 7 Real Time PCR cycler with *Hprt*/*HPRT1* as an internal mRNA control (all Applied Biosystems, *NNAT* Hs00193590_m1; *HPRT1* Hs02800695_m1; *Egfp* Mr04097229_mr; *Mafa* Mm00845209_s1; *Neurod1* Mm01280117_m1; *Nkx6.1* Mm00454962_m1; *Pdx1* Mm0435565_m1; *Nnat* Mm00440480_m1; *Hprt* Mm00446968_m1; *Ins2* Mm00731595_gH; *Slc2a2* (*Glut2*) Mm00446229_m1; *Sst* Mm00436671_m1; *Gcg* Mm00801714_m1).

For RNA sequencing, RNA from FACS-purified cells (four biological replicates each from an individual mouse) was quantified and assessed for integrity (RIN > 9) using a Bioanalyser 2100 and a RNA 6000 pico assay (Agilent Technologies). and 20 ng of RNA was processed for RNA sequencing using a NEBNext Ultra II Directional RNA library Prep Kit for Illumina paired with a Poly(A) mRNA magnetic isolation module and AMPure XP SPRIselect beads (Beckman Coulter), all according to manufacturer's instructions. Libraries were assessed on a Bioanalyser 2100 using a High-Sensitivity DNA assay (Agilent Technologies), with subsequent cDNA quantification using a Quant-iT dsDNA High Sensitivity Assay kit (Thermo Fisher Scientific). Libraries were sequenced using a NextSeq 500 High Output sequencer (Illumina), with 2 x 75 bp length at 50 million reads per sample. Quality assessment of paired end reads was performed using the FASTQC tool (version 0.11.2, http://www.bioinformatics.babraham.ac.uk/projects/fastqc/) and raw reads were aligned to the mouse genome (mm10) using STAR aligner (version 2.7.1a) (83). Gene counts were obtained using STAR and gencode gene annotations (vM25) and differential expression analysis was performed using the DESeq2 Bioconductor package (version 1.32.0) (84). Differentially expressed genes were obtained by comparing NNAT^{+} beta cells, NNAT^{-} beta cells and the non-beta cell fraction. Gene set enrichment analysis was performed using GSEA (version 4.1.0) (85) and the Molecular Signatures Database v7.2.0, with Wald statistical analysis from the differential expression data used to create preranked files as an input to the GSEA preranked analysis.

Bisulphite sequencing

Genomic DNA was extracted from FACS-purified cells using Allprep DNA/RNA/protein mini kits from Qiagen. Sperm cells were lysed using differential extraction, first by incubation in 100 mM Tris-HCl pH 7.5, 200 mM NaCl, 5 mM EDTA, 0.2% SDS, 0.1 mg/mL proteinase K at 55°C for 2h to lyse epithelial cells, followed by pelleting and resuspension of sperm cells in the above lysis buffer plus 10 mM dithiothreitol (DTT) and subsequent DNA extraction using phenol/chloroform/isoamyl alcohol (25:24:1) and standard isopropanol precipitation. Bisulphite conversion and desulphonation was performed using an EZ DNA Methylation-Gold kit from Zymo Research. Eluted DNA was used for amplification of PCR products with primers spanning the *Nnat* promoter (5'-TTTAGGTGGTAAGAGGGTATTTAAGGTA-3' and 5'-AATACATACTCACCTACAACA-3', designed by BiSearch (86) and an EpiTaq hot start kit (TaKaRa Bio). PCR fragments were gel purified (Qiagen), ligated into pJET1.2/blunt using a CloneJET PCR cloning kit (Thermo Scientific) and antibiotic-resistant plasmids prepared in 96 well format using a Wizard SV 96 plasmid DNA purification system (Promega) before Sanger sequencing (Genewiz, now Azenta Life Sciences). Sequencing data was quantified as

percentage of methylated CpGs across 12 clones, using Bisulphite Sequencing DNA Methylation Analysis (BISMA) software (87).

Bioinformatic clustering analysis

Single cell RNA-seq data of islets from chow and HFD mice were downloaded from Gene Expression Omnibus database (accession number GSE110648 (14)). The 78 cells from the chow diet group were used for further analysis and was performed using R package RaceID (88). Mitochondrial genes were removed from the expression matrix prior to downstream analysis and cells were filtered to have at least 5000 transcripts with an expression value of >2. A distance matrix was then constructed using Pearson correlation as the distance metric. A K-nearest neighbour graph layout utilizing the Fruchterman-Rheingold algorithm was performed to cluster cells into different groups, with a value of k = 3. This algorithm also identifies outlier populations, and so a total of six clusters were identified using the clustering method, with differential expression analysis performed comparing individual clusters to all other cells.

Statistical analysis

Data are shown as mean ± SEM in all panels. Data were assessed for normal distribution using the D'Agostino-Pearson normality test with statistical significance between biological groups determined using GraphPad Prism 9 with ANOVA, 2-tailed Student's *t* test (parametric) or Mann-Whitney *U*/Kruskal-Wallis tests (nonparametric) used where appropriate. Bonferroni (or Dunn's as nonparametric equivalent) post hoc tests were utilised to correct for multiple corrections. <5% error probability was considered significant (i.e., $P < 0.05$) and further statistical information, such as *n* numbers and P values, are provided in the figure legends.

Results

Heterogeneous NNAT expression during postnatal development is associated with CpG methylation at *Nnat*

We have previously shown that *Nnat* is crucial for insulin storage and GSIS in the mouse (67). Reanalysis of a published single cell RNA-sequencing dataset of primary mouse beta cells (14) using the scran package (89) (see Methods) identified *Nnat* as amongst the most highly variable genes between individual beta cells (variance = 1.734, FDR = 6.2×10^{13}, mean variance for all transcripts = 0.198). This method avoids artefacts resulting from technical dropouts or of prioritising low abundance genes with large variances due to technical noise. Using a cell clustering algorithm (88) to subdivide individual beta cells based on gene expression from scRNA-sequencing dataset the above we also identified *Nnat* as a highly

significant differentially expression gene between two beta cell clusters (FC = 8.5, FDR = $9.6x10^{-16}$). We confirmed these findings at the protein level using immunofluorescent staining for endogenous NNAT in late postnatal and adult mice (Figure 1A, B). We also observed that NNAT expression is highly dynamic in beta cells across the islet throughout the postnatal stage, transitioning from expression throughout the majority (90.4±3.2%, n = 15 mice) of beta cells at late embryogenesis to a subset (24.4±3.0%, n = 5 mice) of beta cells by P14 (Figure 1A, B). Specific staining for endogenous NNAT was confirmed by the absence of reactivity in pancreatic cryosections from mice with constitutive deletion of the paternal *Nnat* allele (Figure 1A). This subpopulation of NNAT-positive beta cells persisted into adulthood at a similar abundance throughout the islet until six months of age (Figure 1A, B). NNAT expression was not apparent in other islet cell types, including alpha and delta cells at P14. However, NNAT expression was detectable in a small number of alpha and delta cells at E17.5 (Figure 1C, D).

To confirm the above findings using an orthogonal approach, and to facilitate later functional studies, we developed a reporter mouse line expressing eGFP under the control of the *Nnat* promoter and upstream enhancers. Adult reporter mice showed expression of eGFP in a subpopulation (~15% of total) of beta cells (Figure 2A). eGFP expression was allele-specific with expression from the paternal, but not maternal allele, indicating the preservation of *Nnat* imprinting in the reporter (Supplemental Figure 1A, B). Furthermore, eGFP expression was restricted to tissues known to express *Nnat* endogenously (pancreatic islets, hypothalamus) with no evidence of expression in *Nnat*-deficient tissue systems (liver, kidney, muscle) (Supplemental Figure 1A-C). Possession of the transgene did not affect endogenous *Nnat* expression (Supplemental Figure 1B) nor the expression of key beta cell functional genes, and eGFP staining overlapped with endogenous NNAT reactivity (Supplemental Figure 1D, E). Furthermore, through multiple (>6) generations of mice, eGFP reporter expression was silenced via maternal inheritance and re-established through paternal inheritance. Thus, *Nnat* imprinting status for the transgene was restored transgenerationally via the germline. Taken together, these data demonstrate that the *Nnat*-eGFP reporter mouse line mimics endogenous *Nnat* expression.

To isolate and purify beta cells based on NNAT levels, we crossed *Nnat*-eGFP reporter mice with animals expressing *Cre* recombinase under the rat insulin promoter (72) and to transgenic mice expressing a tdTomato reporter downstream of a loxP-flanked stop codon (73). Dispersion of primary adult islets into single cells, and subsequent FACS analysis, verified the presence of $NNAT^+$ and $NNAT^-$ beta cells, with the $NNAT^+$ fraction making up 15.3 ± 1.8% (n = 8 mice) of the total beta cell compartment (Figure 2B, C and Supplemental Figure 2A, B). Collection of FACS-purified $NNAT^+$ and $NNAT^-$ beta cells and subsequent bisulphite

sequencing analysis revealed that CpG methylation at the gametic DMR (known to control monoallelic *Nnat* expression; Introduction) was unchanged (Supplemental Figure 2C-E). Nevertheless, CpG methylation at the *Nnat* promoter was significantly altered across this genomic region, with minimal CpG methylation observed in NNAT$^+$ beta cells (Figure 2D-F).

Recent whole-genome methylation analysis in mouse germ cells has revealed that the *Nnat* promoter region is unmethylated in sperm, and this was confirmed by targeted bisulphite sequencing analysis (Supplemental Figure 2F, G), whereas it is fully methylated in oocytes (90). Overall, our findings indicate that 'classical' imprinting of *Nnat* is unaltered between beta cell subtypes with near binary ('on/off') expression of Neuronatin. However, and overlaying this control, a second DMR at the *Nnat* promoter within the non-imprinted allele dictates beta cell subtype specificity of expression (Figure 2G).

The *de novo* DNA methyltransferase DNMT3A establishes NNAT beta cell subtype specificity

The above data indicate that beta cells transition from a state where the majority (>90%) are NNAT-positive at late embryogenesis to 31.2±3.9% (n = 14 mice) NNAT-positive by postnatal day 7. This is associated with differential CpG methylation at the *Nnat* promoter. To ask whether this apparent transition in the early postnatal period is driven by *de novo* CpG methylation, we assessed endogenous NNAT beta cell immunoreactivity in postnatal mice with conditional deletion of the methyltransferase DNMT3A at the pancreatic progenitor stage (via *Pdx1-Cre*) (15). In control mice, DNMT3A, but not DNMT1 expression, was detected in the majority of beta cells in late embryogenesis (E17.5) but was absent by postnatal day 7 (Figure 3A). NNAT staining in control mice at postnatal (P) day 6 demonstrated expression in a subpopulation of beta cells whereas deletion of DNMT3A resulted in a loss of this heterogenous expression across the islet (Figure 3B, C). These findings demonstrate that *de novo* methylation is likely to drive NNAT restriction across the beta cell complement in the first few days of postnatal life.

NNAT$^+$ and NNAT$^-$ beta cells have distinct transcriptional signatures

After FACS-sorting of primary mouse islet cells as above, we performed RNA-sequencing on the NNAT$^+$ and NNAT$^-$ beta cell fractions. NNAT$^+$ and NNAT$^-$ beta cells displayed high transcriptional overlap and were similar to each other when compared with non-beta endocrine cells from the same islet preparations (Figure 4A). Major beta cell identity markers such as *Ins1*, *Ins2*, *Mafa*, *Slc2a2* (*Glut2*), *Nkx6.1* and *Ucn3* were not differentially expressed (Supplemental Table 1).

We identified 241 (1.8%) and 79 (0.6%) genes that were significantly down- and up-regulated in NNAT$^+$ beta cells, respectively (>2-fold, FDR < 0.01) between the two populations. Genes differentially expressed between NNAT$^+$ and NNAT$^-$ beta cells included several markers of non-beta cell islet lineages (*Pyy*, *Ppy*, *Mafb*, *Sst*), that were lower in the NNAT$^+$ beta cell fraction; genes linked with beta cell heterogeneity and plasticity (*Gpx3*, *Rbp4*), the beta cell immaturity marker *Cd81* (31) and the *Cd24a* antigen (32) (Figure 4B). We did not observe any clear differences between NNAT$^+$ and NNAT$^-$ beta cells in the expression of other imprinted genes known to be functional in the beta cell (*Plagl1*/*ZAC*, *Dlk1*, *Rasgrf1*, *Cdkn1c*, *Grb10* and *Gtl2*/*MEG3*) nor changes in 'disallowed' genes whose expression are known to be restricted in mature functional beta cells (*Hk1*, *Mct1* (*Slc16a1*) and *Ldha*) (91) (Supplemental Table 1). We did not identify changes in transcripts encoding proteins previously demonstrated by others to 'mark' specific beta cell subpopulations such as *Flattop*/*Cfap126* (26), *CD9* and *ST8SIA1* (20), 'virgin' beta cells (via *Ucn3*) (34) or those differentially-expressed in beta cells implicated in the control of Ca^{2+} dynamics ('hubs' (24), and 'leaders' (25, 35)).

Gene set enrichment analysis (GSEA) revealed enrichment of pathways in NNAT$^+$ beta cells including translation initiation, the electron transport chain (ETC), oxidative phosphorylation and signal recognition particle (SRP)-dependent co-translational protein targeting (Figure 4C). Pathways involving genes associated with hepatic nuclear factor 1 alpha (HNF1A) and GLI-similar zinc finger protein family 3 (GLIS3) targets, were reduced in the NNAT$^+$ beta cell fraction (Figure 4D). Thus, transcriptional profiling of NNAT$^+$ beta cells reveal this as a hyper-functional, highly mature beta cell sub-set.

Neuronatin binds to the Signal Peptidase Complex (SPC) in human beta cells, and NNAT deficiency blunts GSIS

Next, we compared the functionality of NNAT$^+$ and NNAT$^-$ beta cells. Whilst this has previously been examined in mouse beta cells (67), no data currently exist for human beta cells. Transient silencing of *NNAT* in human EndoC-βH1 beta cells completely abrogated glucose-stimulated insulin release (Figure 5A-C).

To determine whether this effect may involve altered signal peptidase activity and processing of ER-targeted proteins as observed in mouse beta cells (67), we next applied an unbiased proteomics approach to identify binding partners of NNAT in human beta cells. Immunoprecipitation of endogenous NNAT from EndoC-βH1 beta cells followed by mass spectrometry analysis indicated that NNAT interacted *in cellulo* with subunits of the signal peptidase complex (SPC), SEC11A, SPCS1, SPCS2 and SPCS3 (Figure 5D). To identify the

SPC subunit likely to mediate this interaction we performed by transient knockdown of individual members of the SPC in stable beta cells and subsequent NNAT immunoprecipitation and mass spectrometry. Silencing of *Spcs1* consistently and significantly reduced the abundance of SPC subunits detected in NNAT immunoprecipitates, whereas that of the other complex subunits was without effect. Thus, the NNAT/SPC interaction is likely mediated via SPCS1 (Figure 5E).

NNAT$^+$ beta cells display normal glucose sensing and do not overlap with a highly connected 'hub' cell population

We next asked whether the NNAT$^+$ beta cell component may display altered glucose-induced Ca^{2+} dynamics *versus* the rest of beta cell population, or influence the transmission of Ca^{2+} signals across the islet. To this end, we examined islets from reporter mice with paternally expressed *Nnat*-eGFP. Intracellular Ca^{2+} changes were monitored using the fluorescent, trappable probe Cal-590, and high-speed confocal imaging (76). *Nnat*-GFP$^+$ and *Nnat*-GFP$^-$ cells responded similarly to challenge with high (11 mM) glucose (Figure 6A).

Beta cell-beta cell connectivity, visualised in the topographic representations of connected beta cells and based on the strength of the coactivity between any two cells (Figure 6B) was similarly not different between NNAT$^+$ and NNAT$^-$ populations. Individual beta cells are represented by differently-coloured nodes depending on their coactivity with the rest of the beta cell population within the same optical slice of the islet. Thus, considered across the whole population, the mean Pearson's coefficient of correlation was 0.87 ± 0.01 (Figure 6C), with 14.9% beta cells being significantly connected.

Finally, we determined whether sub-populations of cells implicated in the control of Ca^{2+} dynamics across the islet ('hubs') (24) may be more or less abundant in the NNAT$^+$ population using signal binarisation-based correlation analyses (36). Consistent with earlier studies (24, 25, 29), pooled data over 45 islets uncovered a scale-free network topography (Figure 6D) where a small proportion of beta cells (4.4%) were identified as highly connected 'hub' cells, as assessed by counting the number of beta cells displaying coordinated Ca^{2+} responses with at least 30% of all beta cells (R^2 = 0.31). Of the 45 islets analysed, 34 (75.6%) displayed this same obedience to a power law, and this adherence pertained for both NNAT$^+$ (Figure 6D; R^2 = 0.38) and NNAT$^-$ populations (R^2 = 0.30). Assessed across the whole population of islets, cells could be categorised as belonging to one of four distinct groups (Figure 6E). Of all cells examined, 4.27% were NNAT$^-$ 'hub' cells that displayed coordinated Ca^{2+} responses to an average of 39.0% of all beta cells (Figure 6E, F). Similarly, the fraction of these cells (1.15%, Figure 6E) that were identified as NNAT$^+$ 'hub' cells had an average of 38.3% coactivity with

the remaining cells (Figure 6F). There were no significant differences in connectivity between these two groups (Figure 6F; P = 0.76). Similarly, there were no significant differences in connectivity between $NNAT^+$ and $NNAT^-$ follower cells (P = 0.72). However, when considered within each individual islet, we observed a significantly lower ratio of 'hubs' to 'followers' in $NNAT^+$ *versus* $NNAT^-$ cells (Figure 6G; 2.11% vs 6.39%, respectively, P = 0.0023 by 2-tailed Wilcoxon matched-paired signed rank test).

Whether $NNAT^+$ cells may overlap with 'leader' cells (25, 36) was not explored in the absence of readily identifiable Ca^{2+} waves emanating from a discrete location in the optical sections of the islets studied here.

Discussion

We describe here a novel subgroup of beta cells dictated by transient methylation of a second DMR in the *Nnat* locus. We have previously described the importance of *Nnat* for the normal secretory function of beta cells (67) and from these earlier findings infer that $NNAT^+$ and $NNAT^-$ cells display differences in secretory function. Correspondingly, transcriptomic analysis of purified $NNAT^+$ and $NNAT^-$ beta cells demonstrated that the $NNAT^+$ fraction is enriched for functional pathways including translation initiation, ETC/oxidative phosphorylation pathways and co-translational protein ER membrane targeting. Extending these studies to man, NNAT deficiency in human beta cells severely blunted GSIS, likely via enhancement of signal peptidase-mediated processing via its SPCS1 subunit. Finally, and in line with our previous studies, $NNAT^+$ and $NNAT^-$ cells did not differ in their glucose-induced Ca^{2+} dynamics, although their alignment with a highly-connected group of 'hub' cells differed compared to that of $NNAT^-$ cells. Thus, $NNAT^+$ cells were likelier to belong to the population of 'follower' cells consistent with a role in insulin production rather than glucose detection (24). Correspondingly, the transcriptome of $NNAT^+$ cells does not show enrichment for genes imputed to be enriched in 'hub' cells (25) nor in 'leader' cells (36) which appear to be discrete populations.

It has become increasingly apparent that the epigenome modulates beta cell identity chronically via epigenetic mechanisms such as DNA methylation and post-translational modification of histone proteins (7-14). Furthermore, functional heterogeneity between individual beta cells exists across the pancreatic islet (16-27, 92).

Our work herein provides evidence that the epigenome can control the fate of specific subpopulations of beta cells. CpG methylation plays a crucial role in early beta cell developmental maturation, including the silencing of 'disallowed' genes such as *Hk1*, *Mct1* (*Slc16a1*) and *Ldha* via DNMT3A (13, 91, 93). We demonstrate that islets transition from a state where the majority of beta cells are $NNAT^+$ in late embryogenesis to comprising a restricted subpopulation of $NNAT^+$ beta cells by postnatal (P) day 7. Whether this represents changes at the level of individual beta cells, or the turnover of the $NNAT^+$ population and replacement with a largely $NNAT^-$ population, was not determined in the present studies, and would require investigation using other approaches, including fate mapping (lineage tracing).

Adult $NNAT^+$ beta cells are virtually unmethylated at the *Nnat* promoter whereas robust promoter methylation is apparent in $NNAT^-$ cells. These findings, and the fact that the *Nnat* promoter is differentially methylated between sperm and oocytes (see results), indicates that promoter methylation during this transition is likely to be acquired on the paternal allele (from which *Nnat* is selectively expressed via genomic imprinting). This, however, would need to be

confirmed via allele-specific methylation analysis. Our studies also show that specific deletion of the *de novo* methyltransferase DNMT3A at the pancreatic progenitor stage resulted in partial loss of NNAT-based beta cell heterogeneity. Thus, DNA methylation is a primary driver of restricted NNAT expression in specific beta cells during early maturation.

Might these findings be relevant for the pathogenesis of T2D? Whether demethylation of the second DMR at the *Nnat* locus may occur in T2D is an interesting possibility which remains to be explored. In rodents, even mild hyperglycaemia deregulates *Nnat* expression alongside that of several other critical beta cell identity genes. Moreover, altered CpG methylation is a common observation in diabetic islets at imprinted and non-imprinted *loci* (54-59, 94). A key question is the temporal pattern of these epigenetic events, are they the main driver of altered expression (and therefore function) or does the hyperglycaemia lead to altered expression via other non-epigenetic mechanisms (such as nutrient-sensitive transcription factors) with epigenetic factors acting as a secondary 'reinforcing' step? Indeed, methylation at gametic DMRs is thought to be relatively stable and able to resist nutrient- or physiology-based changes (95, 96). However, 'secondary' imprinting regions have been shown to be more sensitive to environmental changes (15, 97). It will therefore be important to assess nutrient-regulated (i.e. dietary) changes at the *Nnat* second DMR in $NNAT^+$ and $NNAT^-$ beta cell populations across the islet in future studies.

Beta cells expand by replication during the first few days of postnatal life, prior to functional maturation. Transcriptomic data and studies in mouse and human pancreatic beta cells (4, 33, 98) point to an inverse relationship between highly proliferative/partially functional beta cell fractions compared with beta cells with limited proliferative ability but are fully functional. These earlier studies suggest that replication must first slow to allow progression to the mature state. It is still unclear why only a fraction of mature beta cells responds to proliferative stimuli, as well as the precise 'identity' of this beta cell subtype. Previous studies (99-101) have indicated that beta cell proliferation decreases rapidly from postnatal day 9 in mice after which beta cell replication is very low, but stable. It will therefore be crucial to assess replication markers such as *Ki67* and *Mcm2* in $NNAT^+$ vs $NNAT^-$ beta cells in early development and in response to mitogenic-inducing diets (high fat/Western diet) (102).

Our previous findings (67) and the current studies have shown that neuronatin is crucial for GSIS in a cell autonomous manner. Here, we demonstrate postnatal acquisition of beta cell heterogeneity in terms of 'on/off' expression of NNAT from a common $NNAT^+$ beta cell precursor at late embryogenesis. Intact islets from adult mice with *Nnat* deletion display severe lowering of insulin content and GSIS. This finding, alongside the observation that the $NNAT^+$

beta cell fraction is retained well into adulthood, suggests that NNAT$^+$ beta cells play a functional role in the mature islet. Our transcriptomic data comparing NNAT$^+$ vs NNAT$^-$ beta cells shows that the NNAT$^+$ subfraction are highly mature, with comparable levels of key beta cell identity markers *Ins1*, *Ins2*, *Mafa* and *Nkx6.1*, and indeed reduced expression of genes expressed in other islet cells (*Sst*, *Pyy, Ppy* etc (103)). We also observe an enrichment of pathways governing oxidative phosphorylation and translational initiation in NNAT$^+$ beta cells. Consistent with our previous published work (67), the signal peptidase/cotranslational ER apparatus pathway was also enriched in NNAT$^+$ beta cells. Thus, NNAT$^+$ beta cells appear to be a highly mature, and possibly 'hyperfunctional' in terms of insulin synthesis and release.

Previous work (104) showed that the immature vs mature beta cell transcriptome (using the beta cell maturity marker urocortin 3, *Ucn3*) were very similar overall. However, a large number of imprinted genes, including *Nnat*, were significantly downregulated at the late postnatal stage compared with late embryogenesis and the early neonatal stage. Although in general, imprinted gene expression often peaks during early development, our present findings indicate that other imprinted genes with known functional importance in beta cells such as *Plagl1*/*ZAC*, *Dlk1*, *Rasgrf1*, *Cdkn1c*, *Grb10* and *Gtl2*/*MEG3* were not differentially expressed between NNAT$^+$ and NNAT$^-$ beta cells, at least at the RNA level. This suggests that although overall imprinted gene expression across the islet reduces during early development, that of imprinted genes as a whole follows a developmental pattern of reduced expression per cell, whereas for neuronatin this reduced expression is due to restriction toward a subset of (beta) cells.

Imprinted genes often regulate cell proliferation and/or survival, so reduced imprinted gene expression during early beta cell development may be required to balance proliferation vs mature function. The presence of stable heterogenous beta cell populations within the mature islet represents a potential benefit towards fine tuning of insulin secretion (and therefore glycaemia) in response to whole-body nutrient changes. Beta cell hierarchy within the islet has been demonstrated to differ at the level of excitability in terms of Ca^{2+} dynamics to modulate islet insulin secretion (105). Although we did not observe such differences between NNAT$^+$ and NNAT$^-$ beta cells, and so were not identified as 'hub' cells (see above), future work will be required to determine whether these subpopulations differ in terms of their insulin content and specific secretion/exocytotic events.

Consistent with our previous work in rodent beta cells (67), we show that neuronatin binds to the signal peptidase complex in human beta cells, likely via SPCS1. SPCS1 is known to reside on the cytosolic side of the ER membrane and modulate SPC processing via prepeptide translocation (106-108), confirmed recently by electron cryo-microscopy (109), which is likely

to be the site at which NNAT exerts its effect on insulin content. Our previous work demonstrated that primary islets from adult mice (therefore will contain only a subset of beta cells that are NNAT^{+}) with *Nnat* deletion have severely blunted GSIS (67). The experiments described above that would address potential differences in insulin content and exocytosis in specific beta cell subtypes will therefore help determine how loss of *Nnat* expression exerts a major secretory defect across the islet.

Finally, the present work demonstrates how effector genes in pancreatic beta cells such as neuronatin can be controlled at the level of the epigenome, resulting in functional heterogeneity between beta cells. Understanding the contribution of the epigenome to beta cell functional heterogeneity will aid future studies targeting specific beta cell subpopulations, or encouraging them to proliferate or mature. In the future this strategy may provide an attractive therapeutic angle for beta cell replacement or regeneration. Indeed, modulating the expression of imprinted genes in pancreatic beta cells via alterations to the epigenome has been shown to enhance their proliferative capabilities (33, 110, 111). The use of epigenome-modifying compounds (112-114) may thus provide a means of enhancing beta cell function in some settings.

Acknowledgements

Work in the S.J.M. lab was supported by a Wellcome Trust ISSF Fellowship (WREC_PS3619) and a Society for Endocrinology Early Career Grant (WREC_P93206) and Small Equipment Grant (WREC_NCP239). This work was also supported by a Wellcome Trust Project Grant (093082/Z/10/Z) to D.J.W. and funding from the Medical Research Council to D.J.W. (MC-A654-5QB40). G.A.R. was supported by a Wellcome Trust Investigator (WT212625/Z/18/Z) Award, an MRC Programme grant (MR/R022259/1), a John R. Evans Leaders Award from Innovation Canada, an MRC Project Grant (MR/R010676/1), and has received funding from the European Union's Horizon 2020 research and innovation programme via the Innovative Medicines Initiative 2 Joint Undertaking under grant agreement No 115881 (RHAPSODY) to G.A.R.. We thank the LMS/NIHR Imperial Biomedical Research Centre Flow Cytometry Facility for the support. The authors declare no conflict of interest.

Author contributions

SJM and GAR designed the research. VY, FY, KC, EG, NP, AM, SK, ZS, LM, CDL, MS, YH, AM, JE, BP, ND, CW, PS, HK and YA performed experiments and analyses. PH, PM, SD and DJW contributed new reagents/analytical tools. SJM and GAR drafted and/or wrote the manuscript. SJM, DJW and GAR provided funding. SJM and GAR supervised the work.

References

1. Rutter GA, Pullen TJ, Hodson DJ, and Martinez-Sanchez A. Pancreatic beta-cell identity, glucose sensing and the control of insulin secretion. *Biochem J.* 2015;466(2):203-18.
2. Marchetti P, Suleiman M, De Luca C, Baronti W, Bosi E, Tesi M, et al. A direct look at the dysfunction and pathology of the beta cells in human type 2 diabetes. *Semin Cell Dev Biol.* 2020;103:83-93.
3. Salinno C, Cota P, Bastidas-Ponce A, Tarquis-Medina M, Lickert H, and Bakhti M. beta-Cell Maturation and Identity in Health and Disease. *Int J Mol Sci.* 2019;20(21).
4. Stolovich-Rain M, Enk J, Vikesa J, Nielsen FC, Saada A, Glaser B, et al. Weaning triggers a maturation step of pancreatic beta cells. *Dev Cell.* 2015;32(5):535-45.
5. Arda HE, Benitez CM, and Kim SK. Gene regulatory networks governing pancreas development. *Dev Cell.* 2013;25(1):5-13.
6. van Arensbergen J, Garcia-Hurtado J, Maestro MA, Correa-Tapia M, Rutter GA, Vidal M, et al. Ring1b bookmarks genes in pancreatic embryonic progenitors for repression in adult beta cells. *Genes Dev.* 2013;27(1):52-63.
7. Avrahami D, Li C, Zhang J, Schug J, Avrahami R, Rao S, et al. Aging-Dependent Demethylation of Regulatory Elements Correlates with Chromatin State and Improved beta Cell Function. *Cell Metab.* 2015;22(4):619-32.
8. Hoffman BG, Robertson G, Zavaglia B, Beach M, Cullum R, Lee S, et al. Locus co-occupancy, nucleosome positioning, and H3K4me1 regulate the functionality of FOXA2-, HNF4A-, and PDX1-bound loci in islets and liver. *Genome Res.* 2010;20(8):1037-51.
9. Khoo C, Yang J, Weinrott SA, Kaestner KH, Naji A, Schug J, et al. Research resource: the pdx1 cistrome of pancreatic islets. *Mol Endocrinol.* 2012;26(3):521-33.
10. Tennant BR, Robertson AG, Kramer M, Li L, Zhang X, Beach M, et al. Identification and analysis of murine pancreatic islet enhancers. *Diabetologia.* 2013;56(3):542-52.
11. Dhawan S, Georgia S, Tschen SI, Fan G, and Bhushan A. Pancreatic beta cell identity is maintained by DNA methylation-mediated repression of Arx. *Dev Cell.* 2011;20(4):419-29.
12. Szabat M, Lynn FC, Hoffman BG, Kieffer TJ, Allan DW, and Johnson JD. Maintenance of beta-cell maturity and plasticity in the adult pancreas: developmental biology concepts in adult physiology. *Diabetes.* 2012;61(6):1365-71.
13. Dhawan S, Tschen SI, Zeng C, Guo T, Hebrok M, Matveyenko A, et al. DNA methylation directs functional maturation of pancreatic beta cells. *J Clin Invest.* 2015;125(7):2851-60.
14. Lu TT, Heyne S, Dror E, Casas E, Leonhardt L, Boenke T, et al. The Polycomb-Dependent Epigenome Controls beta Cell Dysfunction, Dedifferentiation, and Diabetes. *Cell Metab.* 2018;27(6):1294-308 e7.

15. Parveen N, Wang JK, Bhattacharya S, Cuala J, Singh Rajkumar M, Butler AE, et al. DNA methylation Dependent Restriction of Tyrosine Hydroxylase Contributes to Pancreatic beta-cell Heterogeneity. *Diabetes.* 2023.

16. Salomon D, and Meda P. Heterogeneity and contact-dependent regulation of hormone secretion by individual B cells. *Exp Cell Res.* 1986;162(2):507-20.

17. Bosco D, and Meda P. Actively synthesizing beta-cells secrete preferentially after glucose stimulation. *Endocrinology.* 1991;129(6):3157-66.

18. Kiekens R, In 't Veld P, Mahler T, Schuit F, Van De Winkel M, and Pipeleers D. Differences in glucose recognition by individual rat pancreatic B cells are associated with intercellular differences in glucose-induced biosynthetic activity. *J Clin Invest.* 1992;89(1):117-25.

19. Van Schravendijk CF, Kiekens R, and Pipeleers DG. Pancreatic beta cell heterogeneity in glucose-induced insulin secretion. *J Biol Chem.* 1992;267(30):21344-8.

20. Dorrell C, Schug J, Canaday PS, Russ HA, Tarlow BD, Grompe MT, et al. Human islets contain four distinct subtypes of beta cells. *Nat Commun.* 2016;7:11756.

21. Wang YJ, Schug J, Won KJ, Liu C, Naji A, Avrahami D, et al. Single-Cell Transcriptomics of the Human Endocrine Pancreas. *Diabetes.* 2016;65(10):3028-38.

22. Segerstolpe A, Palasantza A, Eliasson P, Andersson EM, Andreasson AC, Sun X, et al. Single-Cell Transcriptome Profiling of Human Pancreatic Islets in Health and Type 2 Diabetes. *Cell Metab.* 2016;24(4):593-607.

23. Camunas-Soler J, Dai XQ, Hang Y, Bautista A, Lyon J, Suzuki K, et al. Patch-Seq Links Single-Cell Transcriptomes to Human Islet Dysfunction in Diabetes. *Cell Metab.* 2020;31(5):1017-31 e4.

24. Johnston NR, Mitchell RK, Haythorne E, Pessoa MP, Semplici F, Ferrer J, et al. Beta Cell Hubs Dictate Pancreatic Islet Responses to Glucose. *Cell Metab.* 2016;24(3):389-401.

25. Salem V, Silva LD, Suba K, Georgiadou E, Neda Mousavy Gharavy S, Akhtar N, et al. Leader beta-cells coordinate Ca(2+) dynamics across pancreatic islets in vivo. *Nat Metab.* 2019;1(6):615-29.

26. Bader E, Migliorini A, Gegg M, Moruzzi N, Gerdes J, Roscioni SS, et al. Identification of proliferative and mature beta-cells in the islets of Langerhans. *Nature.* 2016;535(7612):430-4.

27. Westacott MJ, Ludin NWF, and Benninger RKP. Spatially Organized beta-Cell Subpopulations Control Electrical Dynamics across Islets of Langerhans. *Biophys J.* 2017;113(5):1093-108.

28. Chabosseau P, Rutter GA, and Millership SJ. Importance of Both Imprinted Genes and Functional Heterogeneity in Pancreatic Beta Cells: Is There a Link? *Int J Mol Sci.* 2021;22(3).

29. Benninger RKP, and Kravets V. The physiological role of beta-cell heterogeneity in pancreatic islet function. *Nat Rev Endocrinol.* 2022;18(1):9-22.
30. Karaca M, Castel J, Tourrel-Cuzin C, Brun M, Geant A, Dubois M, et al. Exploring functional beta-cell heterogeneity in vivo using PSA-NCAM as a specific marker. *PLoS One.* 2009;4(5):e5555.
31. Salinno C, Buttner M, Cota P, Tritschler S, Tarquis-Medina M, Bastidas-Ponce A, et al. CD81 marks immature and dedifferentiated pancreatic beta-cells. *Mol Metab.* 2021;49:101188.
32. Muraro MJ, Dharmadhikari G, Grun D, Groen N, Dielen T, Jansen E, et al. A Single-Cell Transcriptome Atlas of the Human Pancreas. *Cell Syst.* 2016;3(4):385-94 e3.
33. Rodnoi P, Rajkumar M, Moin ASM, Georgia SK, Butler AE, and Dhawan S. Neuropeptide Y expression marks partially differentiated beta cells in mice and humans. *JCI Insight.* 2017;2(12).
34. van der Meulen T, Mawla AM, DiGruccio MR, Adams MW, Nies V, Dolleman S, et al. Virgin Beta Cells Persist throughout Life at a Neogenic Niche within Pancreatic Islets. *Cell Metab.* 2017;25(4):911-26 e6.
35. Kravets V, Dwulet JM, Schleicher WE, Hodson DJ, Davis AM, Pyle L, et al. Functional architecture of pancreatic islets identifies a population of first responder cells that drive the first-phase calcium response. *PLoS Biol.* 2022;20(9):e3001761.
36. Chabosseau P, Yong F, Delgadillo-Silva LF, Lee EY, Melhem R, Li S, et al. Molecular phenotyping of single pancreatic islet leader beta cells by "Flash-Seq". *Life Sci.* 2023:121436.
37. Rutter GA, and Hodson DJ. Beta cell connectivity in pancreatic islets: a type 2 diabetes target? *Cell Mol Life Sci.* 2015;72(3):453-67.
38. Gosak M, Stozer A, Markovic R, Dolensek J, Perc M, Rupnik MS, et al. Critical and Supercritical Spatiotemporal Calcium Dynamics in Beta Cells. *Front Physiol.* 2017;8:1106.
39. Nasteska D, Fine NHF, Ashford FB, Cuozzo F, Viloria K, Smith G, et al. Author Correction: PDX1(LOW) MAFA(LOW) beta-cells contribute to islet function and insulin release. *Nat Commun.* 2021;12(1):4521.
40. Baron M, Veres A, Wolock SL, Faust AL, Gaujoux R, Vetere A, et al. A Single-Cell Transcriptomic Map of the Human and Mouse Pancreas Reveals Inter- and Intra-cell Population Structure. *Cell Syst.* 2016;3(4):346-60 e4.
41. Wojtusciszyn A, Armanet M, Morel P, Berney T, and Bosco D. Insulin secretion from human beta cells is heterogeneous and dependent on cell-to-cell contacts. *Diabetologia.* 2008;51(10):1843-52.
42. Gosak M, Yan-Do R, Lin H, MacDonald PE, and Stozer A. Ca2+ Oscillations, Waves, and Networks in Islets From Human Donors With and Without Type 2 Diabetes. *Diabetes.* 2022;71(12):2584-96.

43. Jetton TL, and Magnuson MA. Heterogeneous expression of glucokinase among pancreatic beta cells. *Proc Natl Acad Sci U S A.* 1992;89(7):2619-23.
44. Heimberg H, De Vos A, Vandercammen A, Van Schaftingen E, Pipeleers D, and Schuit F. Heterogeneity in glucose sensitivity among pancreatic beta-cells is correlated to differences in glucose phosphorylation rather than glucose transport. *EMBO J.* 1993;12(7):2873-9.
45. Katsuta H, Aguayo-Mazzucato C, Katsuta R, Akashi T, Hollister-Lock J, Sharma AJ, et al. Subpopulations of GFP-marked mouse pancreatic beta-cells differ in size, granularity, and insulin secretion. *Endocrinology.* 2012;153(11):5180-7.
46. Xin Y, Dominguez Gutierrez G, Okamoto H, Kim J, Lee AH, Adler C, et al. Pseudotime Ordering of Single Human beta-Cells Reveals States of Insulin Production and Unfolded Protein Response. *Diabetes.* 2018;67(9):1783-94.
47. Surani MA. Genomic imprinting: control of gene expression by epigenetic inheritance. *Curr Opin Cell Biol.* 1994;6(3):390-5.
48. Millership SJ, Van de Pette M, and Withers DJ. Genomic imprinting and its effects on postnatal growth and adult metabolism. *Cell Mol Life Sci.* 2019;76(20):4009-21.
49. Radford EJ, Ferron SR, and Ferguson-Smith AC. Genomic imprinting as an adaptative model of developmental plasticity. *FEBS Lett.* 2011;585(13):2059-66.
50. Peters J. The role of genomic imprinting in biology and disease: an expanding view. *Nat Rev Genet.* 2014;15(8):517-30.
51. Soellner L, Begemann M, Mackay DJ, Gronskov K, Tumer Z, Maher ER, et al. Recent Advances in Imprinting Disorders. *Clin Genet.* 2017;91(1):3-13.
52. Villanueva-Hayes C, and Millership SJ. Imprinted Genes Impact Upon Beta Cell Function in the Current (and Potentially Next) Generation. *Front Endocrinol (Lausanne).* 2021;12:660532.
53. Yamato E, Tashiro F, and Miyazaki J. Microarray analysis of novel candidate genes responsible for glucose-stimulated insulin secretion in mouse pancreatic beta cell line MIN6. *PLoS One.* 2013;8(4):e61211.
54. Prokopenko I, Poon W, Magi R, Prasad BR, Salehi SA, Almgren P, et al. A central role for GRB10 in regulation of islet function in man. *PLoS Genet.* 2014;10(4):e1004235.
55. Kameswaran V, Golson ML, Ramos-Rodriguez M, Ou K, Wang YJ, Zhang J, et al. The Dysregulation of the DLK1-MEG3 Locus in Islets From Patients With Type 2 Diabetes Is Mimicked by Targeted Epimutation of Its Promoter With TALE-DNMT Constructs. *Diabetes.* 2018;67(9):1807-15.
56. Dayeh T, Volkov P, Salo S, Hall E, Nilsson E, Olsson AH, et al. Genome-wide DNA methylation analysis of human pancreatic islets from type 2 diabetic and non-diabetic donors identifies candidate genes that influence insulin secretion. *PLoS Genet.* 2014;10(3):e1004160.

57. Lawlor N, George J, Bolisetty M, Kursawe R, Sun L, Sivakamasundari V, et al. Single-cell transcriptomes identify human islet cell signatures and reveal cell-type-specific expression changes in type 2 diabetes. *Genome Res.* 2017;27(2):208-22.

58. Fadista J, Vikman P, Laakso EO, Mollet IG, Esguerra JL, Taneera J, et al. Global genomic and transcriptomic analysis of human pancreatic islets reveals novel genes influencing glucose metabolism. *Proc Natl Acad Sci U S A.* 2014;111(38):13924-9.

59. Volkmar M, Dedeurwaerder S, Cunha DA, Ndlovu MN, Defrance M, Deplus R, et al. DNA methylation profiling identifies epigenetic dysregulation in pancreatic islets from type 2 diabetic patients. *EMBO J.* 2012;31(6):1405-26.

60. Kong A, Steinthorsdottir V, Masson G, Thorleifsson G, Sulem P, Besenbacher S, et al. Parental origin of sequence variants associated with complex diseases. *Nature.* 2009;462(7275):868-74.

61. El Hajj N, Schneider E, Lehnen H, and Haaf T. Epigenetics and life-long consequences of an adverse nutritional and diabetic intrauterine environment. *Reproduction.* 2014;148(6):R111-20.

62. Soubry A, Schildkraut JM, Murtha A, Wang F, Huang Z, Bernal A, et al. Paternal obesity is associated with IGF2 hypomethylation in newborns: results from a Newborn Epigenetics Study (NEST) cohort. *BMC Med.* 2013;11:29.

63. Soubry A, Murphy SK, Wang F, Huang Z, Vidal AC, Fuemmeler BF, et al. Newborns of obese parents have altered DNA methylation patterns at imprinted genes. *Int J Obes (Lond).* 2015;39(4):650-7.

64. Reik W, and Walter J. Genomic imprinting: parental influence on the genome. *Nat Rev Genet.* 2001;2(1):21-32.

65. Ferguson-Smith AC. Genomic imprinting: the emergence of an epigenetic paradigm. *Nat Rev Genet.* 2011;12(8):565-75.

66. John RM, and Lefebvre L. Developmental regulation of somatic imprints. *Differentiation.* 2011;81(5):270-80.

67. Millership SJ, Da Silva Xavier G, Choudhury AI, Bertazzo S, Chabosseau P, Pedroni SM, et al. Neuronatin regulates pancreatic beta cell insulin content and secretion. *J Clin Invest.* 2018;128(8):3369-81.

68. Vrang N, Meyre D, Froguel P, Jelsing J, Tang-Christensen M, Vatin V, et al. The imprinted gene neuronatin is regulated by metabolic status and associated with obesity. *Obesity (Silver Spring).* 2010;18(7):1289-96.

69. Dalgaard K, Landgraf K, Heyne S, Lempradl A, Longinotto J, Gossens K, et al. Trim28 Haploinsufficiency Triggers Bi-stable Epigenetic Obesity. *Cell.* 2016;164(3):353-64.

70. Millership SJ, Tunster SJ, Van de Pette M, Choudhury AI, Irvine EE, Christian M, et al. Neuronatin deletion causes postnatal growth restriction and adult obesity in 129S2/Sv mice. *Mol Metab.* 2018;18:97-106.

71. Yang CH, Fagnocchi L, Apostle S, Wegert V, Casani-Galdon S, Landgraf K, et al. Independent phenotypic plasticity axes define distinct obesity sub-types. *Nat Metab.* 2022;4(9):1150-65.

72. Herrera PL. Adult insulin- and glucagon-producing cells differentiate from two independent cell lineages. *Development.* 2000;127(11):2317-22.

73. Luche H, Weber O, Nageswara Rao T, Blum C, and Fehling HJ. Faithful activation of an extra-bright red fluorescent protein in "knock-in" Cre-reporter mice ideally suited for lineage tracing studies. *Eur J Immunol.* 2007;37(1):43-53.

74. Kaneda M, Okano M, Hata K, Sado T, Tsujimoto N, Li E, et al. Essential role for de novo DNA methyltransferase Dnmt3a in paternal and maternal imprinting. *Nature.* 2004;429(6994):900-3.

75. Hingorani SR, Petricoin EF, Maitra A, Rajapakse V, King C, Jacobetz MA, et al. Preinvasive and invasive ductal pancreatic cancer and its early detection in the mouse. *Cancer Cell.* 2003;4(6):437-50.

76. Georgiadou E, Muralidharan C, Martinez M, Chabosseau P, Akalestou E, Tomas A, et al. Mitofusins Mfn1 and Mfn2 Are Required to Preserve Glucose- but Not Incretin-Stimulated beta-Cell Connectivity and Insulin Secretion. *Diabetes.* 2022;71(7):1472-89.

77. Akalestou E, Suba K, Lopez-Noriega L, Georgiadou E, Chabosseau P, Gallie A, et al. Intravital imaging of islet Ca(2+) dynamics reveals enhanced beta cell connectivity after bariatric surgery in mice. *Nat Commun.* 2021;12(1):5165.

78. Tschen SI, Dhawan S, Gurlo T, and Bhushan A. Age-dependent decline in beta-cell proliferation restricts the capacity of beta-cell regeneration in mice. *Diabetes.* 2009;58(6):1312-20.

79. Schindelin J, Arganda-Carreras I, Frise E, Kaynig V, Longair M, Pietzsch T, et al. Fiji: an open-source platform for biological-image analysis. *Nat Methods.* 2012;9(7):676-82.

80. Ravassard P, Hazhouz Y, Pechberty S, Bricout-Neveu E, Armanet M, Czernichow P, et al. A genetically engineered human pancreatic beta cell line exhibiting glucose-inducible insulin secretion. *J Clin Invest.* 2011;121(9):3589-97.

81. Maechler P, and Wollheim CB. Mitochondrial glutamate acts as a messenger in glucose-induced insulin exocytosis. *Nature.* 1999;402(6762):685-9.

82. Tyanova S, Temu T, and Cox J. The MaxQuant computational platform for mass spectrometry-based shotgun proteomics. *Nat Protoc.* 2016;11(12):2301-19.

83. Dobin A, Davis CA, Schlesinger F, Drenkow J, Zaleski C, Jha S, et al. STAR: ultrafast universal RNA-seq aligner. *Bioinformatics.* 2013;29(1):15-21.

84. Love MI, Huber W, and Anders S. Moderated estimation of fold change and dispersion for RNA-seq data with DESeq2. *Genome Biol.* 2014;15(12):550.

85. Subramanian A, Tamayo P, Mootha VK, Mukherjee S, Ebert BL, Gillette MA, et al. Gene set enrichment analysis: a knowledge-based approach for interpreting genome-wide expression profiles. *Proc Natl Acad Sci U S A.* 2005;102(43):15545-50.

86. Tusnady GE, Simon I, Varadi A, and Aranyi T. BiSearch: primer-design and search tool for PCR on bisulfite-treated genomes. *Nucleic Acids Res.* 2005;33(1):e9.

87. Rohde C, Zhang Y, Reinhardt R, and Jeltsch A. BISMA--fast and accurate bisulfite sequencing data analysis of individual clones from unique and repetitive sequences. *BMC Bioinformatics.* 2010;11:230.

88. Herman JS, Sagar, and Grun D. FateID infers cell fate bias in multipotent progenitors from single-cell RNA-seq data. *Nat Methods.* 2018;15(5):379-86.

89. Lun AT, McCarthy DJ, and Marioni JC. A step-by-step workflow for low-level analysis of single-cell RNA-seq data with Bioconductor. *F1000Res.* 2016;5:2122.

90. Jima DD, Skaar DA, Planchart A, Motsinger-Reif A, Cevik SE, Park SS, et al. Genomic map of candidate human imprint control regions: the imprintome. *Epigenetics.* 2022;17(13):1920-43.

91. Pullen TJ, Huising MO, and Rutter GA. Analysis of Purified Pancreatic Islet Beta and Alpha Cell Transcriptomes Reveals 11beta-Hydroxysteroid Dehydrogenase (Hsd11b1) as a Novel Disallowed Gene. *Front Genet.* 2017;8:41.

92. Wang G, Chiou J, Zeng C, Miller M, Matta I, Han JY, et al. Integration of single-cell multiomic measurements across disease states with genetics identifies mechanisms of beta cell dysfunction in type 2 diabetes. *bioRxiv.* 2nd January 2023; doi: https://doi.org/10.1101/2022.12.31.522386.

93. Ni Q, Sun J, Wang Y, Wang Y, Liu J, Ning G, et al. mTORC1 is required for epigenetic silencing during beta-cell functional maturation. *Mol Metab.* 2022;64:101559.

94. Ebrahimi AG, Hollister-Lock J, Sullivan BA, Tsuchida R, Bonner-Weir S, and Weir GC. Beta cell identity changes with mild hyperglycemia: Implications for function, growth, and vulnerability. *Mol Metab.* 2020;35:100959.

95. Ivanova E, Chen JH, Segonds-Pichon A, Ozanne SE, and Kelsey G. DNA methylation at differentially methylated regions of imprinted genes is resistant to developmental programming by maternal nutrition. *Epigenetics.* 2012;7(10):1200-10.

96. Radford EJ, Isganaitis E, Jimenez-Chillaron J, Schroeder J, Molla M, Andrews S, et al. An unbiased assessment of the role of imprinted genes in an intergenerational model of developmental programming. *PLoS Genet.* 2012;8(4):e1002605.

97. Van de Pette M, Abbas A, Feytout A, McNamara G, Bruno L, To WK, et al. Visualizing Changes in Cdkn1c Expression Links Early-Life Adversity to Imprint Mis-regulation in Adults. *Cell Rep.* 2017;18(5):1090-9.

98. Puri S, Roy N, Russ HA, Leonhardt L, French EK, Roy R, et al. Replication confers beta cell immaturity. *Nat Commun.* 2018;9(1):485.

99. Qiu WL, Zhang YW, Feng Y, Li LC, Yang L, and Xu CR. Deciphering Pancreatic Islet beta Cell and alpha Cell Maturation Pathways and Characteristic Features at the Single-Cell Level. *Cell Metab.* 2017;25(5):1194-205 e4.

100. Wang YJ, Golson ML, Schug J, Traum D, Liu C, Vivek K, et al. Single-Cell Mass Cytometry Analysis of the Human Endocrine Pancreas. *Cell Metab.* 2016;24(4):616-26.

101. Teta M, Long SY, Wartschow LM, Rankin MM, and Kushner JA. Very slow turnover of beta-cells in aged adult mice. *Diabetes.* 2005;54(9):2557-67.

102. Moulle VS, Ghislain J, and Poitout V. Nutrient regulation of pancreatic beta-cell proliferation. *Biochimie.* 2017;143:10-7.

103. DiGruccio MR, Mawla AM, Donaldson CJ, Noguchi GM, Vaughan J, Cowing-Zitron C, et al. Comprehensive alpha, beta and delta cell transcriptomes reveal that ghrelin selectively activates delta cells and promotes somatostatin release from pancreatic islets. *Mol Metab.* 2016;5(7):449-58.

104. Blum B, Hrvatin S, Schuetz C, Bonal C, Rezania A, and Melton DA. Functional beta-cell maturation is marked by an increased glucose threshold and by expression of urocortin 3. *Nat Biotechnol.* 2012;30(3):261-4.

105. Benninger RK, Hutchens T, Head WS, McCaughey MJ, Zhang M, Le Marchand SJ, et al. Intrinsic islet heterogeneity and gap junction coupling determine spatiotemporal Ca(2)(+) wave dynamics. *Biophys J.* 2014;107(11):2723-33.

106. Kalies KU, and Hartmann E. Membrane topology of the 12- and the 25-kDa subunits of the mammalian signal peptidase complex. *J Biol Chem.* 1996;271(7):3925-9.

107. Antonin W, Meyer HA, and Hartmann E. Interactions between Spc2p and other components of the endoplasmic reticulum translocation sites of the yeast Saccharomyces cerevisiae. *J Biol Chem.* 2000;275(44):34068-72.

108. Zhang R, Miner JJ, Gorman MJ, Rausch K, Ramage H, White JP, et al. A CRISPR screen defines a signal peptide processing pathway required by flaviviruses. *Nature.* 2016;535(7610):164-8.

109. Liaci AM, Steigenberger B, Telles de Souza PC, Tamara S, Grollers-Mulderij M, Ogrissek P, et al. Structure of the human signal peptidase complex reveals the determinants for signal peptide cleavage. *Mol Cell.* 2021;81(19):3934-48 e11.

110. Sanchez-Parra C, Jacovetti C, Dumortier O, Lee K, Peyot ML, Guay C, et al. Contribution of the Long Noncoding RNA H19 to beta-Cell Mass Expansion in Neonatal and Adult Rodents. *Diabetes.* 2018;67(11):2254-67.
111. Ou K, Yu M, Moss NG, Wang YJ, Wang AW, Nguyen SC, et al. Targeted demethylation at the CDKN1C/p57 locus induces human beta cell replication. *J Clin Invest.* 2019;129(1):209-14.
112. Ganesan A, Arimondo PB, Rots MG, Jeronimo C, and Berdasco M. The timeline of epigenetic drug discovery: from reality to dreams. *Clin Epigenetics.* 2019;11(1):174.
113. Astro V, and Adamo A. Epigenetic Control of Endocrine Pancreas Differentiation in vitro: Current Knowledge and Future Perspectives. *Front Cell Dev Biol.* 2018;6:141.
114. Montalvo-Casimiro M, Gonzalez-Barrios R, Meraz-Rodriguez MA, Juarez-Gonzalez VT, Arriaga-Canon C, and Herrera LA. Epidrug Repurposing: Discovering New Faces of Old Acquaintances in Cancer Therapy. *Front Oncol.* 2020;10:605386.

Figures

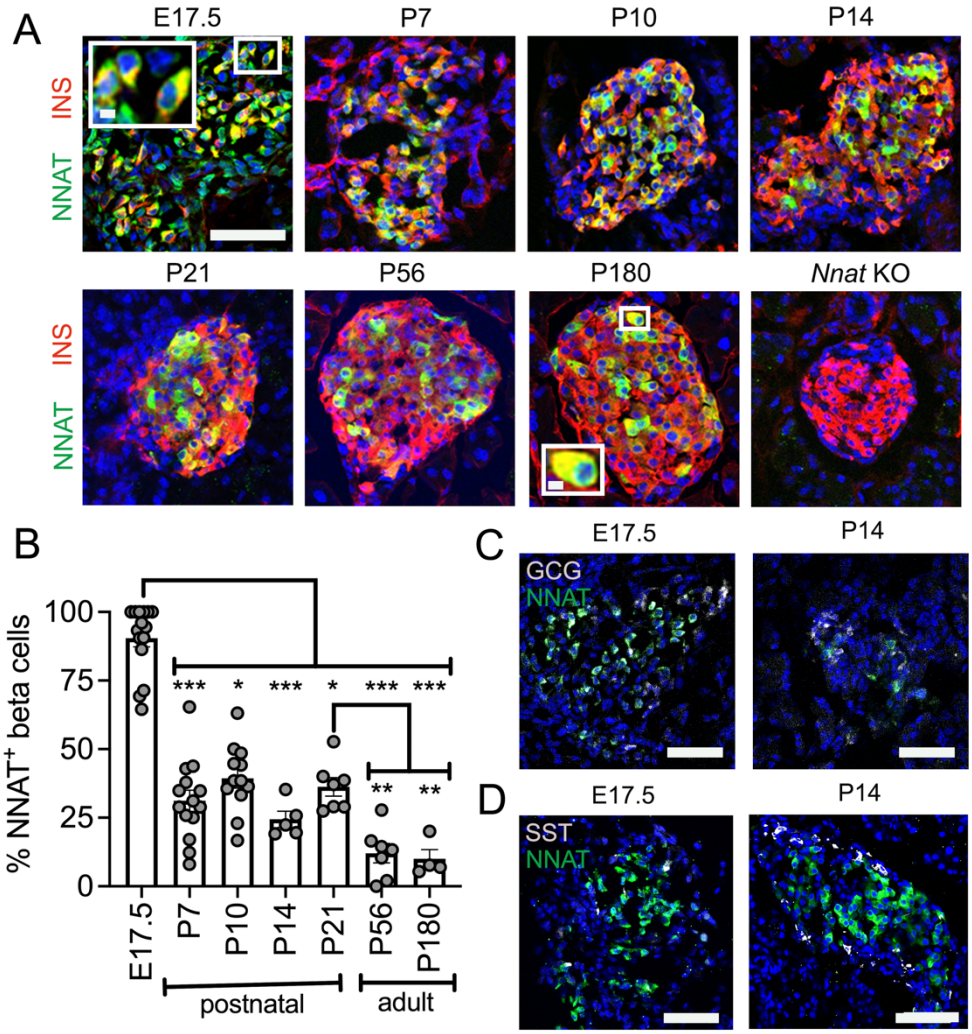

Figure 1. A subpopulation of NNAT$^+$ beta cells develop during the early postnatal period in mice. (A) Representative confocal microscopy of pancreatic cryosections from wild type mice on a C57BL/6J background of developmental stages from embryonic day 17.5 (E17.5) through the postnatal (P) period into adulthood. Sections were immunostained with antibodies against endogenous neuronatin (NNAT, green) and insulin (INS, red). Nuclei are visualised with DAPI and sections from P56 mice with constituent deletion of *Nnat* were used as an immunostaining control. Scale bar = 100μm (inset = 10μm) (n = 4-15 mice per timepoint, Kruskal-Wallace test with Dunn's multiple comparisons). **(B)** Quantification of NNAT$^+$ beta cells from images shown in A, expressed as NNAT/INS co-positive cells as a percentage of total INS-positive cells. **(C, D)** Representative confocal microscopy of pancreatic cryosections as in A from E17.5 and postnatal (P) day 14 mice (n = 15 and n = 5 mice, respectively) immunostained with antibodies against endogenous neuronatin (NNAT, green) and GCG (C) or SST (D) (both grey). Scale bar = 100μm. * $P < 0.05$, ** $P < 0.01$, *** $P < 0.001$.

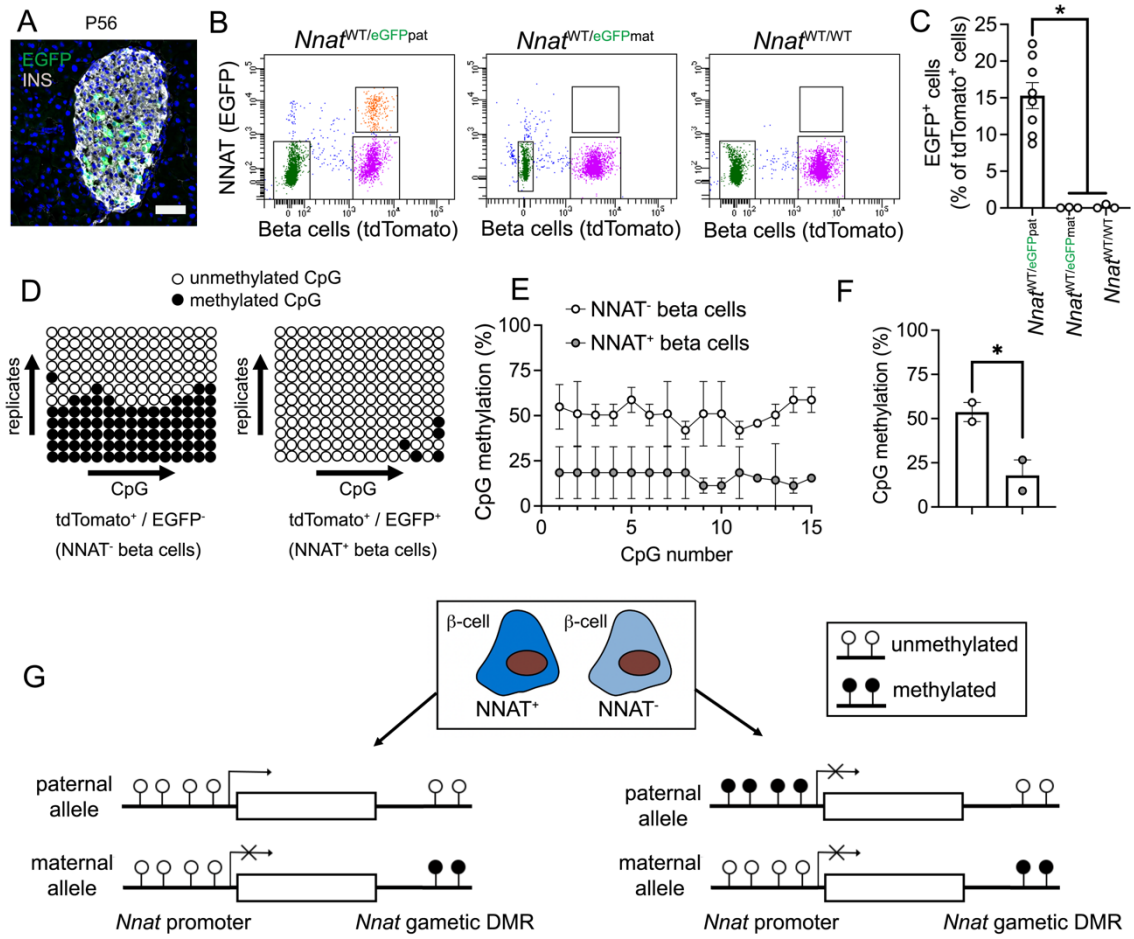

Figure 2. Beta cell heterogeneity of NNAT expression is associated with changes in CpG methylation at the *Nnat* promoter. (**A**) Representative confocal microscopy of pancreatic cryosections from P56 mice with *Nnat*-driven EGFP expression from the paternal allele (*Nnat*$^{WT/eGFPpat}$) (n = 7 mice). Sections were immunostained with antibodies against EGFP (green) and insulin (INS, grey). Nuclei are visualised with DAPI. Scale bar = 50μm. (**B**) Separation of dispersed primary islet cells by FACS from reporter mice with insulin-driven expression of tdTomato (to label beta cells) and *Nnat*-driven EGFP expression from the paternal (*Nnat*$^{WT/eGFPpat}$), or maternal (*Nnat*$^{WT/eGFPmat}$) allele or wild type (*Nnat*$^{WT/WT}$) at this locus (representative image of one dispersed islet preparation, each from a single mouse) (n = 8, 3 and 3 mice, respectively, Kruskal-Wallace test with Dunn's multiple comparisons). (**C**) Quantification of data in B expressed as percentage of EGFP/tdTomato co-positive primary islet cells. (**D**) Representative bisulphite analysis of CpG methylation at the *Nnat* promoter in FACS-purified islet cell populations from B (n = 2 *Nnat*$^{WT/eGFPpat}$ mice with paternally expressed *Nnat*-driven EGFP, n = 12 clones each). Closed circles = methylated CpG, open circles = unmethylated CpG. (**E, F**) Quantification of data in D expressed as percentage CpG methylation across the *Nnat* promoter at individual CpGs (E) and across the entire *Nnat* promoter (F) (Wilcoxon matched-pairs signed rank test). (G) Schematic summarising level of

CpG methylation at the *Nnat* promoter and gametic DMR in NNAT^{+} vs NNAT^{-} beta cells. * P < 0.05.

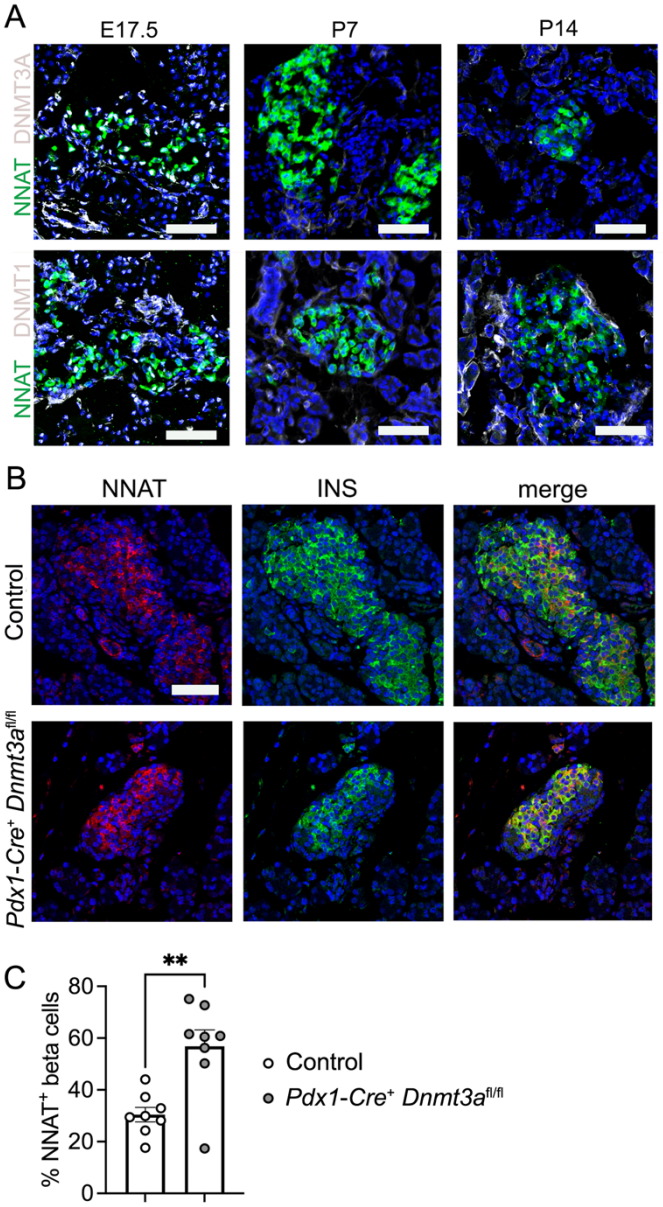

Figure 3. Postnatal restriction of NNAT in a subset of beta cells is driven by the *de novo* methyltransferase, DNMT3A. (**A**) Representative confocal microscopy of pancreatic cryosections from *Nnat*$^{WT/eGFPpat}$ mice at embryonic (E) day 17.5 and postnatal (P) day 7 and 14 (n = 15 and 14 mice, respectively). Sections were immunostained with antibodies against endogenous neuronatin (NNAT, green) and DNMT3A or DNMT1 (both grey). Nuclei are visualised with DAPI. Scale bar = 50μm. (**B**) Representative confocal microscopy of pancreatic cryosections from mice with conditional deletion of DNMT3A under the control of the *Pdx1* promoter (*Pdx1-Cre*$^{+}$ *Dnmt3a*$^{fl/fl}$) vs control (*Pdx1-Cre*$^{-}$ *Dnmt3a*$^{fl/fl}$) mice at postnatal (P) day 6. Sections were immunostained with antibodies against endogenous neuronatin (NNAT, red) and insulin (INS, green). (**C**) Quantification of NNAT^{+} beta cells from images shown in B, expressed as NNAT/INS co-positive cells as a percentage of total INS-positive cells. Nuclei are visualised with DAPI. Scale bar = 50μm (n = 8 islets from two mice per genotype, unpaired Students t test, ** P < 0.01).

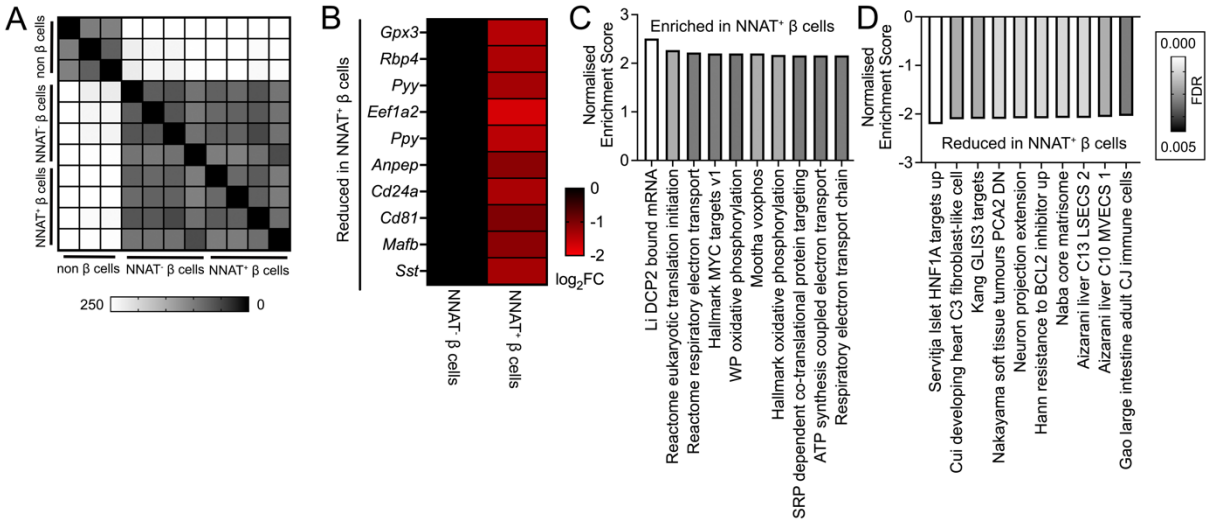

Figure 4. NNAT$^+$ and NNAT$^-$ beta cells are transcriptionally distinct. (**A**) Correlation matrix of differentially expressed genes between NNAT$^+$ and NNAT$^-$ beta cells as assessed by RNA-sequencing analysis (n = 4 FACS-purified populations from individual mouse islet preparations). (**B**) Heatmap of top 10 most differentially expressed genes reduced in NNAT$^+$ beta cells compared with NNAT$^-$ beta cells. (**C, D**) Gene set enrichment analysis (GSEA) showing categories significantly enriched (C) and reduced (D) in NNAT$^+$ (vs NNAT$^-$) beta cells.

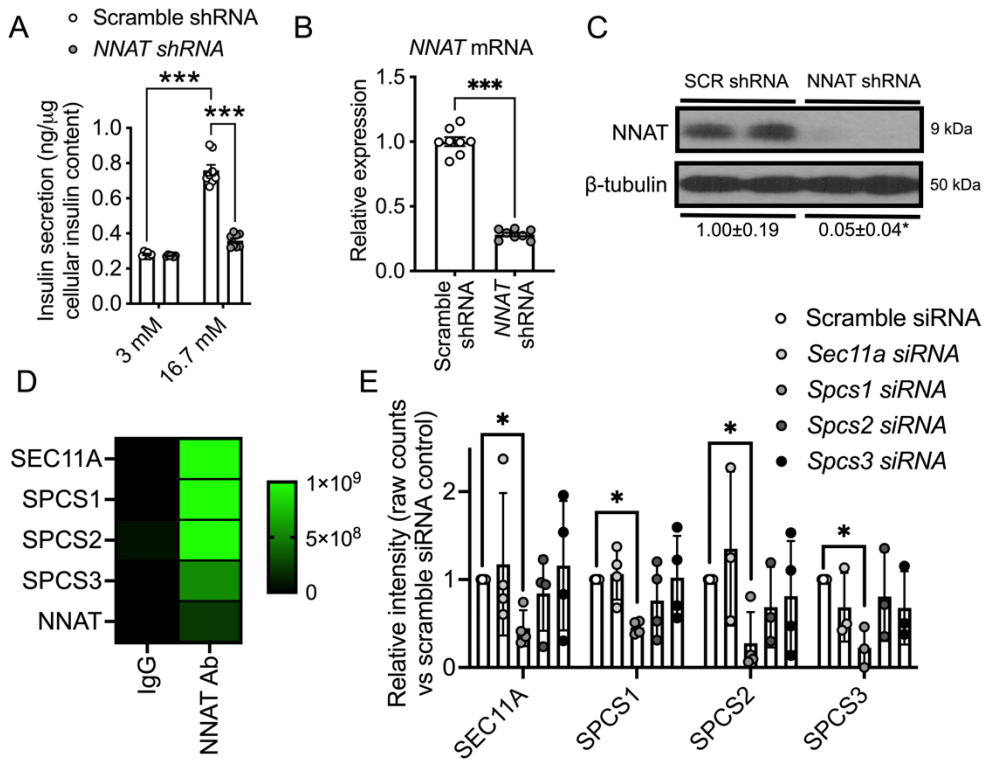

Figure 5. NNAT deficiency in human beta cells reduces insulin secretion likely by modulating the SPC apparatus through SPCS1. (**A**) GSIS analysis at low (3 mM) and high (16.7 mM) glucose in human EndoC-βH1 beta cells following 72h lentiviral-mediated shRNA knockdown of neuronatin with data expressed as of insulin secreted into culture media as a percentage of total cellular insulin content (n = 8 independent cultures per group, two-way ANOVA with Sidak's multiple corrections test). (**B, C**) RT-PCR (n = 8, unpaired Student's t test) and Western blot (n = 4, Mann-Whitney U test) analysis of neuronatin expression in EndoC-βH1 beta cells after transient *NNAT* silencing as in A. Western blotting analysis of NNAT protein levels shown via a representative blot of two independent experiments. β-tubulin was used as a loading control. Mean values for band intensities in multiple experiments quantified by densitometry are shown below the panel, expressed relative to scramble (SCR) shRNA controls. (**D**) Heatmap from affinity purification/mass spectrometry (AP/MS) analysis showing co-immunoprecipitation of signal peptidase complex subunits with endogenous NNAT in human EndoC-βH1 beta cells using antibodies against NNAT (NNAT Ab) vs control IPs with rabbit immunoglobulins (IgG). (E) INS1E cells transiently transfected with siRNA targeting subunits of the signal peptidase complex followed by NNAT immunoprecipitation as above and detection of signal peptidase complex components by affinity purification/mass spectrometry (AP/MS) analysis, with relative protein abundance measured vs scramble siRNA controls (n = 4 independent cultures per group, Kruskal-Wallace test with Dunn's multiple comparisons). * P < 0.05, *** P < 0.001, **** P < 0.0001).

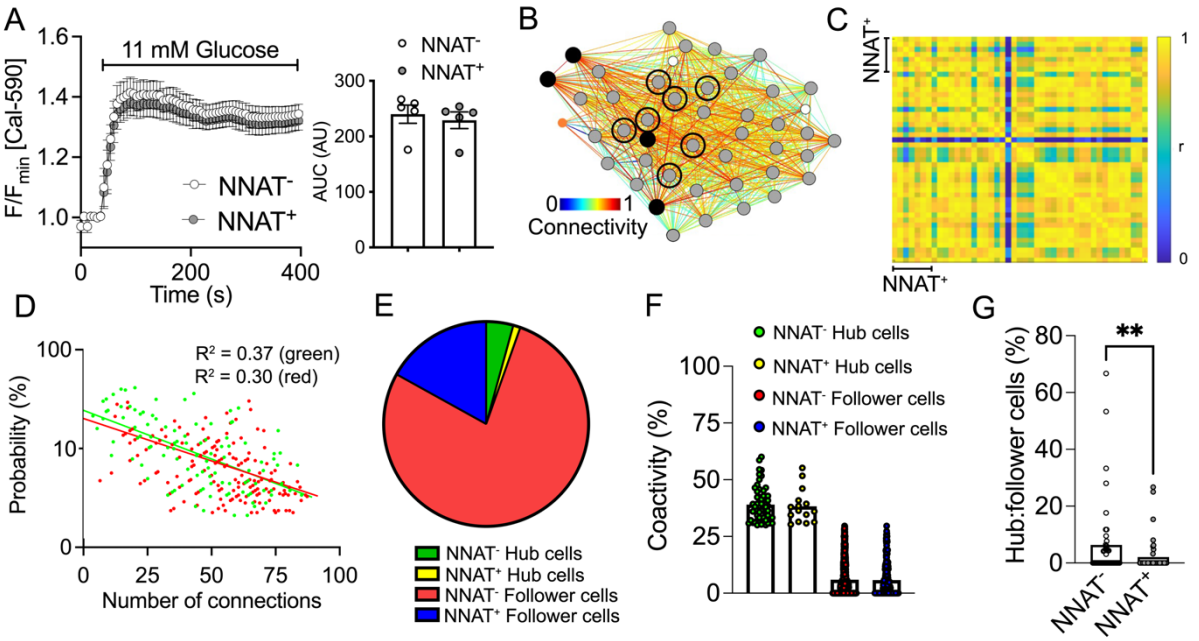

Figure 6. NNAT$^+$ beta cells show unaltered glucose-induced Ca^{2+} dynamics but are de-enriched for highly connected 'hub' cells within individual islets. (**A**) Ca^{2+} bound Cal-590 fluorescence in response to high glucose (11 mM) in NNAT$^-$ and NNAT$^+$ cells from primary islets from *Nnat*$^{WT/eGFPpat}$ reporter mice expressed as normalised intensity over time (F / F$_{min}$) (n = 61 islets total from five mice per genotype, inset shows quantification of area under the curve (AUC), P = 0.063, Wilcoxon matched-pairs signed rank test). (**B**) Representative cartesian map of beta cells with colour coded lines connecting cells according of the strength of coactivation (colour coded R values from 0 to 1, blue to red). Beta cells are represented by differently coloured nodes depending on their coactivity with the other beta cells, where black nodes indicate coactivity with ≥80% of the remaining beta cells, while grey and white nodes represent coactivity with ≥60% and ≥40%, respectively. Nodes circled with a solid black line indicate NNAT$^+$ cells. (**C**) Representative heatmaps depicting connectivity strength (r) of all cell pairs (colour coded r values from 0 to 1, blue to yellow). (**D**) Log-log graphs of beta cell-beta cell connectivity distribution: 4.40% of beta cells coactivated with at least 30% of the rest of the beta cells, identifying 'hub' cells that display an obedience to a power-law distribution, whereby few beta cells host 30-100% of the connections to the rest of the beta cell population. NNAT$^+$ cells are represented by green circles while NNAT$^-$ cells are represented by red circles (45 islets total using primary islet preparations, each from an individual *Nnat*$^{WT/eGFPpat}$ reporter mouse). (**E**) Categorisation of beta cells based on data from D: 4.27% of all beta cells are defined as NNAT$^-$ 'hub' cells; 1.15% as NNAT$^+$ 'hub' cells; 17.0% as NNAT$^+$ 'follower cells'; 77.6% as NNAT$^-$ 'follower' cells. (**F**) Percentage coactivity of beta cells between all cells. Identified 'hub' cells displayed coordinated Ca^{2+} responses to an average of 39.0% of all beta

cells. NNAT$^+$ cells that were identified to be 'hub' cells displayed coordinated Ca^{2+} responses to an average of 38.3% of all beta cells; connectivity between NNAT$^-$ and NNAT$^+$ 'hub' cells (P = 0.76, unpaired Students t test). Both NNAT$^-$ and NNAT$^+$ 'follower' cells had significantly fewer coordinated Ca^{2+} responses compared to both pure hub cell populations, at averages of 5.79% and 5.98% respectively (P < 0.001, unpaired Students t test). There were no significant differences in connectivity between NNAT$^-$ and NNAT$^+$ 'follower' cells (P = 0.72, unpaired Students t test). (**G**) The proportion of cells designated as 'hub' cells vs 'follower' cells in both the NNAT$^-$ and NNAT$^+$ populations assessed in each of 45 islets, ** P < 0.01, Wilcoxon matched-pairs signed rank test).